1991-06

Energy threshold for laser induced breakdown on a metal surface under high and ultra high vacuum conditions.

Gedik, Abdullah

Monterey, California. Naval Postgraduate School

NAVAL POSTGRADUATE SCHOOL
Monterey, California

THESIS

ENERGY THRESHOLD FOR LASER INDUCED BREAKDOWN ON A METAL SURFACE UNDER HIGH AND ULTRA HIGH VACUUM CONDITIONS

by

Abdullah Gedik

June 1991

Thesis Advisor: F. R. Schwirzke

REPORT DOCUMENTATION PAGE

1a. REPORT SECURITY CLASSIFICATION: UNCLASSIFIED	1b. RESTRICTIVE MARKINGS
2a. SECURITY CLASSIFICATION AUTHORITY	3. DISTRIBUTION/AVAILABILITY OF REPORT: Approved for public release; distribution is unlimited
2b. DECLASSIFICATION/DOWNGRADING SCHEDULE	
4. PERFORMING ORGANIZATION REPORT NUMBER(S)	5. MONITORING ORGANIZATION REPORT NUMBER(S)
6a. NAME OF PERFORMING ORGANIZATION: Department of Physics, Naval Postgraduate School; 6b. OFFICE SYMBOL (*if applicable*): 33	7a. NAME OF MONITORING ORGANIZATION: Naval Postgraduate School
6c. ADDRESS (*City, State, and ZIP Code*): Monterey, CA 93943-5000	7b. ADDRESS (*City, State, and ZIP Code*): Monterey, CA 93943-5000
8a. NAME OF FUNDING/SPONSORING ORGANIZATION; 8b. OFFICE SYMBOL (*if applicable*)	9. PROCUREMENT INSTRUMENT IDENTIFICATION NUMBER
8c. ADDRESS (*City, State, and ZIP Code*)	10. SOURCE OF FUNDING NUMBERS: PROGRAM ELEMENT NO. / PROJECT NO. / TASK NO. / WORK UNIT ACCESSION NO.

11. TITLE (*Include Security Classification*)
ENERGY THRESHOLD FOR LASER INDUCED BREAKDOWN ON A METAL SURFACE UNDER HIGH AND ULTRA HIGH VACUUM CONDITIONS

12. PERSONAL AUTHOR(S): Abdullah Gedik

13a. TYPE OF REPORT	13b. TIME COVERED FROM TO	14. DATE OF REPORT (*Year, Month, Day*)	15. PAGE COUNT
Master's Thesis		June 1991	39

16. SUPPLEMENTARY NOTATION: The views expressed in this thesis are those of the author and do not reflect the official policy or position of the Department of Defense or the United States Government.

17. COSATI CODES			18. SUBJECT TERMS (*Continue on reverse if necessary and identify by block number*)
FIELD	GROUP	SUB-GROUP	Laser induced breakdown, Plasma onset, Unipolar Arcing, Cascaded breakdown, Multi photon ionization, Thermal runaway

19. ABSTRACT (*Continue on reverse if necessary and identify by block number*)

Unipolar arcing is the primary breakdown process when a powerful laser pulse interacts with a target surface. The unipolar arc model assumes that the initial ionization occurs in desorbed gas layers. To check this experimentally a metal surface was illuminated under different vacuum conditions. The experiments were conducted at 10^{-4}, 10^{-6} and 10^{-8} torr vacuum. A neodymium:glass laser of wavelength 1.06 μm in the Q-switched mode was utilized. Type 304, polished, stainless steel plates were used as targets. Results confirmed that higher laser energy was needed to trigger the laser induced breakdown at lower pressures.

20. DISTRIBUTION/AVAILABILITY OF ABSTRACT: ☒ UNCLASSIFIED/UNLIMITED ☐ SAME AS RPT. ☐ DTIC USERS	21. ABSTRACT SECURITY CLASSIFICATION: UNCLASSIFIED	
22a. NAME OF RESPONSIBLE INDIVIDUAL: F.R. Schwirzke	22b. TELEPHONE (*Include Area Code*): (408) 646-2431	22c. OFFICE SYMBOL: PH/Sw

Approved for public release; distribution is unlimited

Energy Threshold for Laser Induced Breakdown
on a Metal Surface
under High and Ultra High Vacuum Conditions

by

Abdullah Gedik
Captain, Turkish Army
B.S., Turkish Military Academy, 1981
M.S., Electrical Engineering, Middle East Technical University, 1985

Submitted in partial fulfillment of the
requirements for the degree of

MASTER OF SCIENCE IN PHYSICS

from the

NAVAL POSTGRADUATE SCHOOL
June 1991

K. E. Woehler, Chairman,
Department of Physics

ABSTRACT

Unipolar arcing is the primary breakdown process when a powerful laser pulse interacts with a target surface. The unipolar arc model assumes that the initial ionization occurs in desorbed gas layers. To check this experimentally a metal surface was illuminated under different vacuum conditions. The experiments were conducted at 10^{-4}, 10^{-6}, and 10^{-8} torr vacuum. A neodymium:glass laser of wavelength 1.06 μm in the Q-switched mode was utilized. Type 304, polished, stainless steel plates were used as targets. Results confirmed that higher laser energy was needed to trigger the laser induced breakdown at lower pressures.

TABLE OF CONTENTS

I. INTRODUCTION 1

II. BACKGROUND 4

A. LASER INDUCED BREAKDOWN AND UNIPOLAR ARCING 4

B. MONOLAYER FORMATION 10

III. EXPERIMENTAL DESIGN 12

A. EQUIPMENT 12

1. Laser System 12

2. Energy Measurement 14

3. Ultra High Vacuum Chamber 18

B. PROCEDURES 19

1. Target Preparation 19

2. Plasma Onset 20

IV. EXPERIMENTAL RESULTS 21

A. PLASMA FORMATION 21

B. PLASMA ONSET 21

CONCLUSIONS 29

LIST OF REFERENCES 30

INITIAL DISTRUBITION LIST 31

I. INTRODUCTION

Soon after the development of the ruby laser, experiments were carried out which showed that by bringing a laser beam to a tight focus, one could cause the breakdown of air. Like the bright spot seen when an electrical discharge occurs between two electrodes, a bright spot would be visible due to breakdown caused by a strong laser pulse. Various experiments with gases, solids, and liquids have been performed to determine the cause of this breakdown, to measure the threshold of power levels to ignite a spark, to determine the effects of wavelength, pulse shape and pulse duration on different type of materials. Experiments were conducted with the high power lasers available: 10.6μm (CO_2), 3.8 (DF), 2.7 (HF), 1.06 (Neodymium, glass), and 0.69μm (ruby). Recent developments made possible the use of higher frequency and higher power lasers such as dye-laser systems and excimer lasers. [Ref. 1]

Laser-induced breakdown can be defined as the generation of an ionized gas by the laser pulse. The experimental breakdown criterion generally used is the observation of a glow or a flash at the region hit by the laser pulse . Other diagnostic means are: measurement of the transmission of a probe beam travelling parallel to the surface or of the main beam by drilling a pin hole through the material, observation of the dramatic decrease in the metal surface reflectivity during the pulse, line emission by ionized species, radiometry of surface, and direct measurement of electron concentration by electrostatic probes. [Ref. 1]

As described in Reference 1, there are two main mechanisms for electron generation and growth. The first mechanism is the absorption of laser radiation by electrons while they collide with neutrals in the focal volume. If the electron has sufficient energy, it can ionize the gas or solid by the reaction

$$e^- + M \rightarrow 2e^- + M^+ \tag{1}$$

By this reaction the electron concentration will increase exponentially, a phenomenon called "cascaded breakdown." The situation is comparable to the dielectric breakdown of gases, liquids, and solids. In order to have this process work, two conditions must be satisfied: (1) the presence of an initial electron in the focal volume and (2) the electrons should gain an energy greater than the band gap of the solid or the ionization energy of the gas. The source of the initial electrons will be discussed later. [Ref. 1]

The second mechanism is called "Multi Photon Ionization", (MPI). It involves the simultaneous absorption of a sufficient number of photons by an atom or a molecule in a gas to cause its ionization, or to eject an electron from the valence to the conduction band in a solid. The reaction for MPI is

$$M + mh\nu \rightarrow M^+ + e^- \tag{2}$$

If ε_i is the band gap or ionization potential, the number of simultaneous photons m must exceed the integer part of $(\varepsilon_i/h\nu+1)$. The rate of ionization in a laser beam of irradiance I is proportional to I^m. The electron density, for constant I, increases linearly with time, if recombination is neglected. Multiphoton ionization is important only for short wavelengths ($\lambda < 1\mu m$). For most gases, the ionization potentials are larger than 10 eV.

It is highly improbable to have simultaneous absorption of 100 or more photons from a CO_2 laser ($h\nu$=0.1eV) to ionize one molecule. [Ref. 1]

Both mechanisms require high laser irradiances such as 10^8 W/cm^2 for gaseous breakdown. For solids the power level required is less, 10^6 W/cm^2. If the solid is transparent at the laser frequency, then the power level required can be even less due to the self focusing effect. If the solid is absorbing at the given laser frequency then there is a third mechanism which is called "thermal runaway." When the solid absorbs the radiation, it evaporates and a shock is driven into the surrounding air. Absorption of laser radiation by the electrons in the surrounding air and behind the shock front results in the heating of the vapor and the shocked air. This leads to more electrons created by thermal generation. The increasing electron number causes more absorption and so on. Hence, we have a thermal runaway situation. In order to have thermal runaway, the vapor and the shocked air should have enough electrons initially to enable the gas to be heated up during the laser pulse. [Ref. 1]

This thesis study is focused on the laser induced breakdown on metallic surfaces. The material used for the experiment is type 304 stainless steel. The breakdown of the metallic surface by a high power (6 joules, 1.06μm wavelength) laser beam was observed for different vacuum conditions. The power required for such a breakdown was measured.

II. BACKGROUND

A. LASER INDUCED BREAKDOWN AND UNIPOLAR ARCING

The following excerpt is taken directly from References 2 and 9 with the permission of the author. He supervised this thesis study as well.

"When a sufficiently powerful laser pulse is incident on a target surface in vacuum, breakdown takes place on the surface and a plasma layer is formed [Ref. 2]". "The initial breakdown phase may be characterized by localized desorption of contaminants from laser heated spots on the surface of a metal. Microprojections or whiskers, dust particles, absorbing inclusions, metal grain boundaries etc., can serve as such spots. If the electric field due to the laser radiation is high enough, field emission of electrons takes place. Whiskers, adsorbates and dust can further enhance the field emission of electrons. While most of the laser light will be reflected from a metal surface, some absorption occurs within the skin depth. Localized heating, enhanced electric fields, and the emission of electrons lead to desorption of a few monolayers within a few ns forming an expanding high density neutral gas cloud as indicated in Figure 2.1. Electron heating and ionization of neutral particles will preferentially occur at a distance $\lambda/4$ from the surface where for normal incidence the first maximum of the electric field occurs due to the superposition of the incidence wave and the wave reflected on the metal surface." [Ref. 9]

"The electrons in the laser heated plasma have a considerable higher thermal velocity than ions. Therefore, the electrons would tend to vacate the plasma at a higher

rate leaving the plasma with a net positive charge and hence with a positive potential with respect to the target surface. Debye shielding causes the main potential variation be present in a sheath which is of the order of the Debye length in thickness $\lambda_D = (\varepsilon_0 kT_e/ne^2)^{1/2}$. The self-adjusting feature of the sheath ensures that the electron and ion fluxes to the surface are equal thus maintaining the quasi-neutrality of the plasma. The plasma assumes a positive potential with respect to the wall as given by the floating potential

$$V_f = \frac{kT_e}{2e} \ln\left(\frac{M_i}{2\pi m_e}\right) \tag{3}$$

The average electric field in the sheath is approximately

$$E \approx \frac{V_f}{\lambda_D} = (n_e kT_e)^{1/2} (1/4\epsilon_0)^{1/2} \ln(M_i/2\pi m_e) \tag{4}$$

E approaches zero near the plasma boundary and assumes its maximal value at the surface." [Ref. 2]

"Unipolar arcing represents a discharge form which easily leads to explosive plasma formation. Unipolar arcing begins if E in the sheath increases enough to ignite and sustain an arc. The initial step will be field emission from surface spots. Electron emission from non-uniform or contaminated surfaces requires fields of the order 10^5 V/cm. Clean smooth metal surfaces require fields of 10^7 V/cm. The Fowler Nordheim theory describes the field emission current from a clean cold surface. Taking into account enhancement factors β, the enhanced field emission current density increases with E where c_1 and c_2 are factors which are approximately constant. ϕ is the work function.

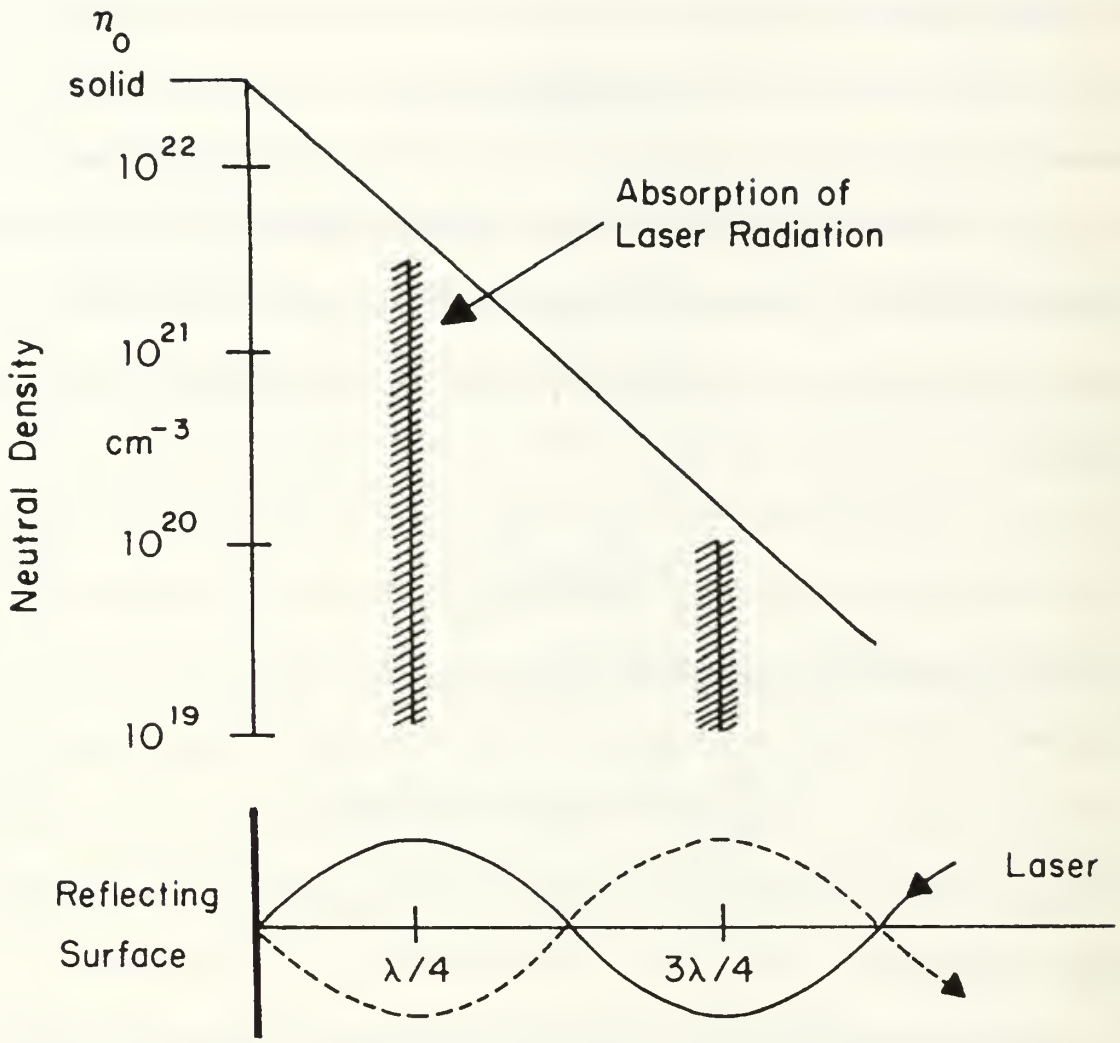

Figure 2.1. Absorption of laser radiation near a reflecting surface. The neutral density gradient in front of the surface is caused by blow-off of surface material. [Ref. 9]

$$j \sim (c_1 \beta^2 E^2/\phi)\exp(-c_2 \phi^{3/2}/\beta E) \tag{5}$$

The enhancement factor β depends on the shape and chemical composition of the emission site. The existence of whiskers, for example Figure 2.2, implies that the field at the tip is considerably enhanced, $E_{tip} = \beta E$, relative to the average field E which exists in the space charge sheath. Average electric fields of $E \geq 10^5$ V/cm in the sheath lead

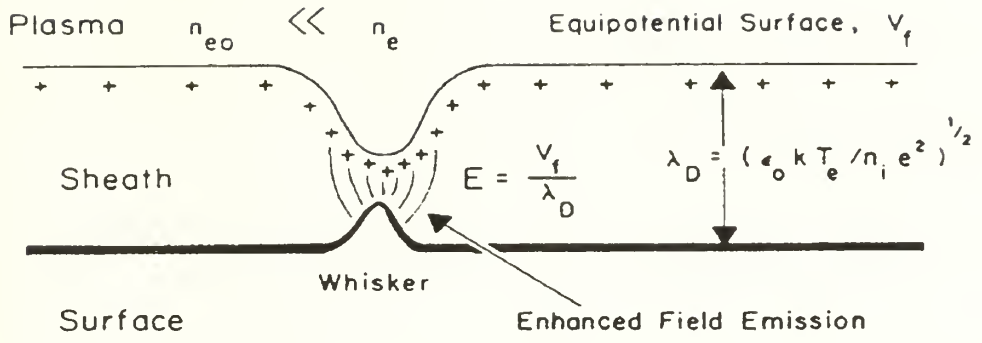

Figure 2.2. The enhanced electric field emission from a whisker [Ref. 2]

to enhanced field emission if enhancement factors of $\beta \approx 10^2$-10^3 exist." [Ref. 2]

"Localized ion density variations strongly influence the enhancement factor too. Electrons emitted from the whisker will be accelerated by the sheath electric field. If the sheath potential is larger than the ionization potential the emitted electrons can ionize neutrals and the plasma density increases. A relatively slowly expanding cloud of neutrals is produced by desorption and evaporation of impurities (gases, hydrocarbon, water, etc.) if a laser heated plasma contacts a surface. The enhanced E at the whisker will not only increase the electron emission but also the ion flux from the plasma to these spots. The increased ion bombardment and recombination rates lead to a locally increased surface temperature at the spot. This in turn leads to locally enhanced desorption of gases, and finally the evaporation of neutral metal atoms into the sheath of plasma. The localized surface heating is also enhanced by the lower thermal conduction rate from projections and dielectric inclusions compared to the surrounding metal surface. The combined effect of the enhanced electron and neutral emission from the surface spots leads to an increased ionization rate producing fairly immobile ions thus increasing the

local plasma density and the sheath electric field. This in turn further increases the field emission current and this the ionization rate and so on until an arc ignites. The electric field energy density or the plasma pressure respectively

$$(1/2)\epsilon_0 E^2=(n_e kT_e)(1/8)[\ln(M_i/2\pi m_e)]^2 \tag{6}$$

become so large that the plasma is literally drilling a hole into the surface." [Ref. 2]

"The local increase in the plasma density over the cathode spot in addition to decreasing the sheath width and increasing the electric field strength across the sheath, creates a radial pressure gradient, ∇P, over the cathode spot. This pressure (density) gradient forms an electric field, E(r) in the radial direction tangential to the surface

$$E(r)=-(kT_e/e)(1/n)(dn/dr) \tag{7}$$

The faster migration of the electrons from the higher density region lowers the sheath potential in a ringlike area surrounding the higher plasma pressure region directly over the cathode spot,

$$\Delta V(r)=(kT_e/e)\ln(n_e(r)/n_{eo}) \tag{8}$$

The ratio of the maximum plasma density above the cathode spot to the unperturbed plasma density can easily be of the order (n_e/n_{eo}) 10^3 or larger. The arc current loop is completed by the return flow of the larger number of electrons from the high energy tail in the Maxwellian distribution that can now overcome the lowered sheath potential surrounding the cathode spot and reach the surface. Figure 2.3 is a diagram of this unipolar arc model. The ejection of plasma jets from the cathode craters leads to the

filamentary structures of laser produced plasmas which have often been observed." [Ref. 2]

This study investigates the dependence of the breakdown process on the amount of adsorbed gases. The model assumes that ionization occurs first in desorbed gases. The amount of the desorbed gases depends on the pressure in the chamber.

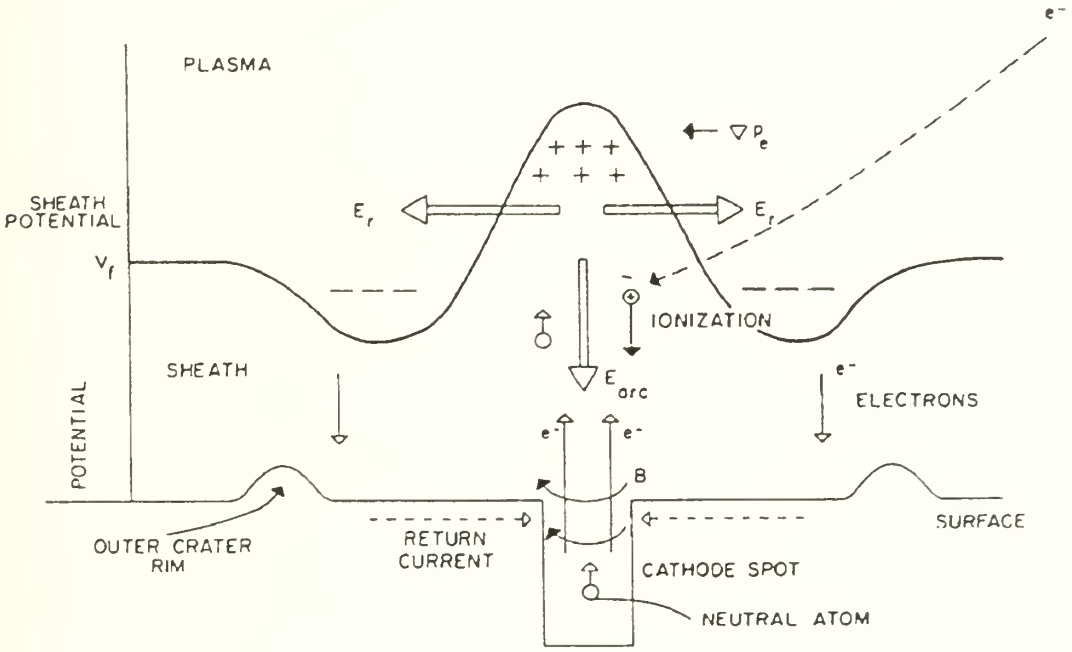

Figure 2.3. Unipolar arc model. B is the magnetic field surrounding the arc current. [Ref. 2]

B. MONOLAYER FORMATION

The border between high vacuum and ultra high vacuum is usually taken as a few 10^{-8} torr. The gas density in room temperature in the ultra high vacuum (UHV, 10^{-8} torr) is very low ($3.3x10^{8}$ cm^{-3}, at atmospheric pressure it is $2.5x10^{19}$ cm^{-3}) [Ref. 10]. After a laser shot, molecules or atoms from the metal surface are blown off. In time, molecules and atoms will be coming back onto the metal surface slowly forming a monolayer or, if there is enough time between the shots, multilayers. With the assumption that every atom or molecule which arrives at the metal surface stays there, a convenient rule of thumb formula for monolayer formation time, τ, is [Ref. 3]

$$\tau = (2.4/p)x10^{-6} \tag{9}$$

where τ is in seconds, p is in torr. Depending on the background pressure, ultrahigh vacuum monolayer formation time is of the order of minutes or even hours. But, for higher pressures (10^{-6}, 10^{-4} torr) the time can be rather short. In Figure 2.4 we give a plot of number of monolayers versus time for various pressures.

In the vacuum chamber used for this work, the gases which were present were: H_2O, N_2, H_2 and, CO_2. In this experiment the onset of plasma formation was studied as a function of background pressure and laser power.

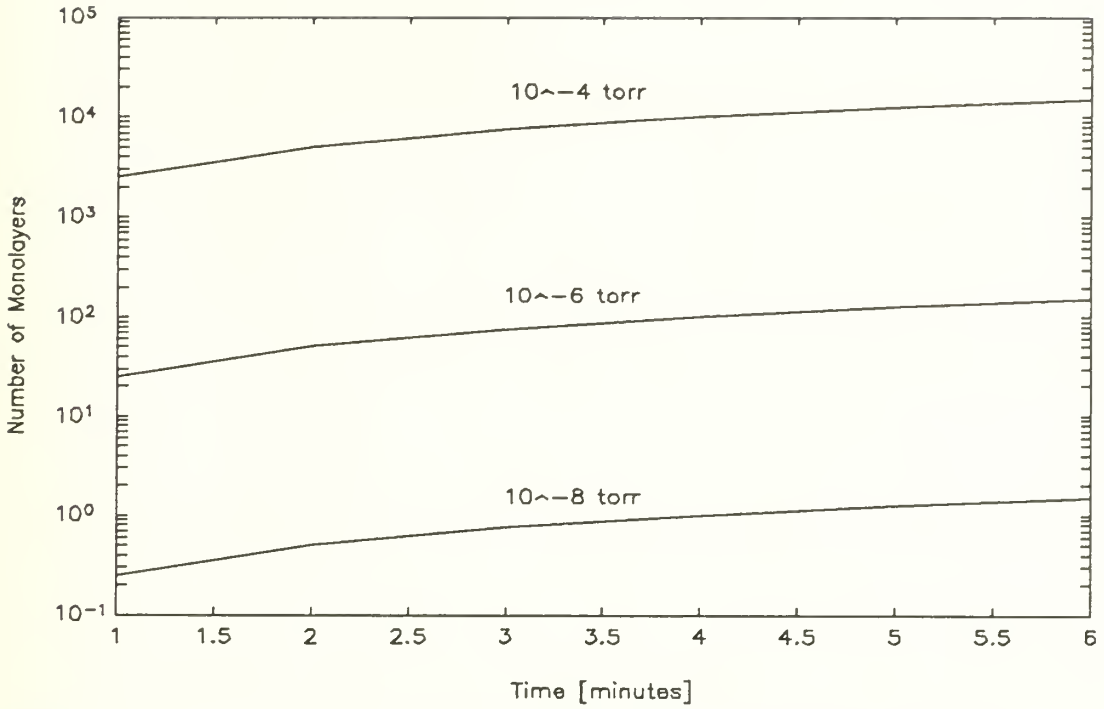

Figure 2.4. Monolayer formation on a metal surface at various pressures.

III. EXPERIMENTAL DESIGN

A. EQUIPMENT

In this experiment the laser was focused onto a target in a vacuum chamber and the laser energy was monitored. Breakdown light emission was observed with a polaroid still camera.

The equipment used in this experiment to determine the onset of plasma formation included an evacuated test chamber, a neodymium-glass laser (1.06 μm), a laser energy measurement set up, several beam splitters, a focusing lens, an ionization gauge, a mass spectrometer, and a polaroid camera. Figure 3.1 is a schematic of the Nd:glass laser, the vacuum chamber and the other equipment used.

1. Laser System

The laser used was a KORAD K-1500 Q-switched neodymium-doped glass laser [Ref. 4]. The nominal energy output of the laser was 6 joules and the average beam pulse half width was 30 nanoseconds. This short pulse width was achieved by utilizing a pockels cell between the oscillator and the rear reflector. The various energy levels on the target were achieved by using several neutral density filters between the laser and the target. After filtering, the laser beam was focused by a focusing lens of 25 cm focal length. The target was placed behind the focal point of the lens, such that the incoming laser beam with a 285.0 mm^2 cross section was focused down to 19.1 mm^2 on the target surface. The reason of focusing the laser beam to a smaller cross section was the

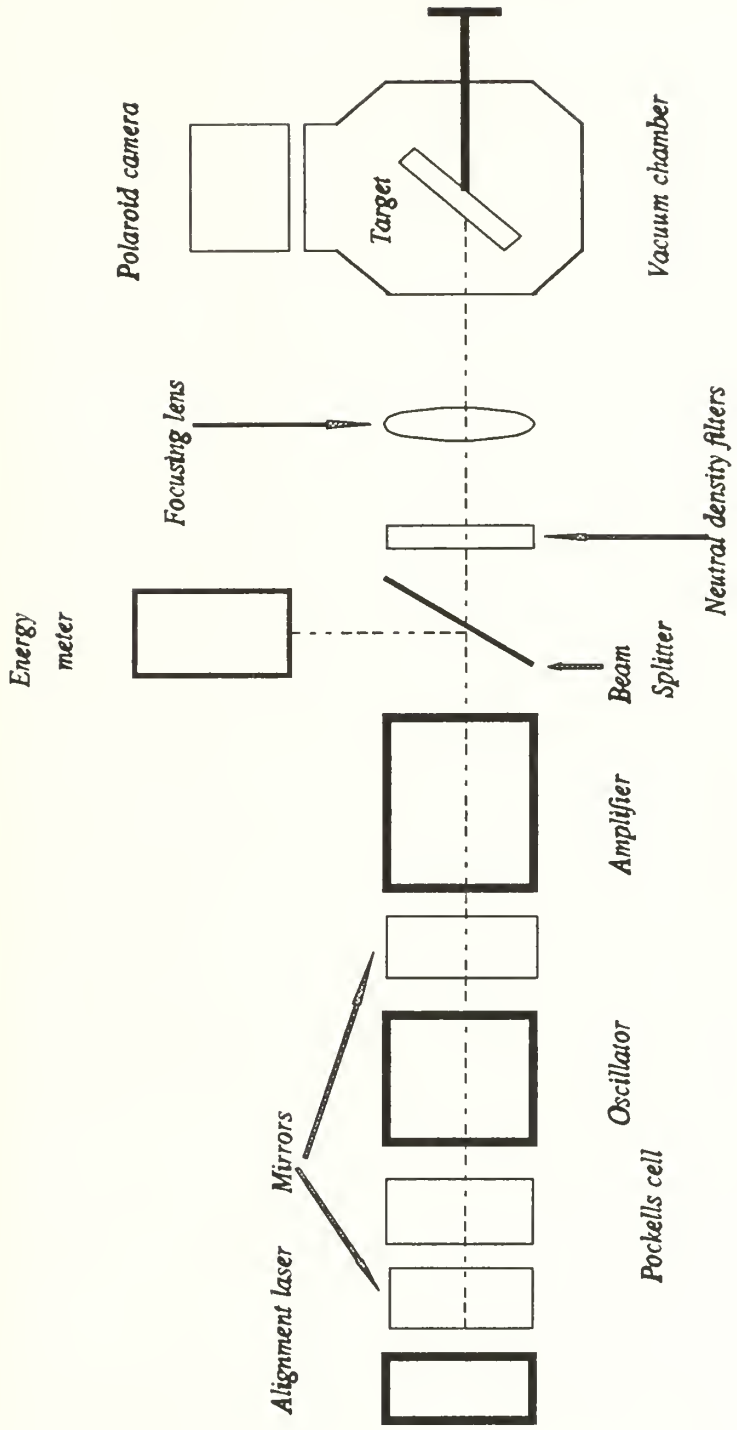

Figure 3.1. Schematic of pulsed laser and vacuum chamber set up.

following: The laser beam had a circular cross section and its intensity over the cross section was not uniform. It had some "hot spots", spots with a higher light intensity. With the unfocused laser beam it was difficult to monitor the onset of breakdown and plasma formation with the polaroid camera. Since the energy of the whole beam was being measured, it was not possible to determine the peak power of these hot spots which could cause plasma formation easier than the other areas of the beam. Also, it was easier to determine the onset of breakdown, by looking at the pictures of a smaller surface. Another advantage of focusing the laser beam was maintaining the same target over a number of shots. To choose another spot on the target, it was rotated by rotating the probe from outside. Changing the target was a time consuming procedure. After replacing the target, it took about two days to pump down to ultra high vacuum. The energy of the laser beam was measured by the set up explained in the following section.

2. Energy Measurement

For this experiment a fast energy meter was not available for the 1.06 μm wavelength of the Nd:glass laser. A KORAD Model K-J laser calorimeter [Ref. 5] with a micro voltmeter in combination with an hp type 7035B chart plotter were used. A portion of the main laser beam was sent to the calorimeter via an 8% beam splitter. As shown in Figure 3.2, the output of the calorimeter was connected to the voltmeter, and the output of the voltmeter was fed to the plotter. The resulting chart was used to determine the energy as explained in reference 5. The only handicap of this system was that it was not time efficient. It would require 10 minutes to determine the energy of the previous shot, and after several shots the calorimeter had to be cooled down. This was

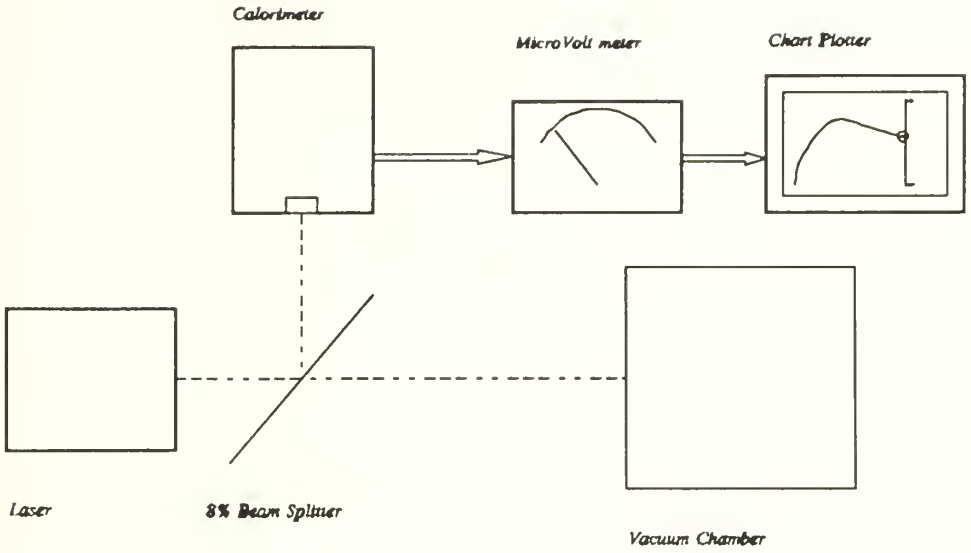

Figure 3.2. Arrangement for laser energy measurement using a calorimeter.

not practical and was not proper for the experiment because, it was needed to have shots as fast as the laser permitted in order not to let too many contaminants get back to the target surface. Hence, the calorimeter was used to calibrate the output of an Opto-electronics Series PD-40 Ultra High Speed photodetector [Ref. 6]. As shown in Figure 3.3, another 8% beam splitter was used for the photodetector to monitor the laser beam. Since the aperture of the diode was smaller than the laser beam size, a focusing lens was used to scale the beam down. The output of the photodiode was displayed on a Tektronix Model 7104 oscilloscope. The oscilloscope was triggered externally by the output of a Lasermetrics Series 3117 High Speed Photodetector which detected the laser beam via a third beam splitter. The pulse on the screen was recorded by using a Tektronix DCS01 Digitizing Camera System [Ref. 7]. A typical pulse captured by that system is shown in

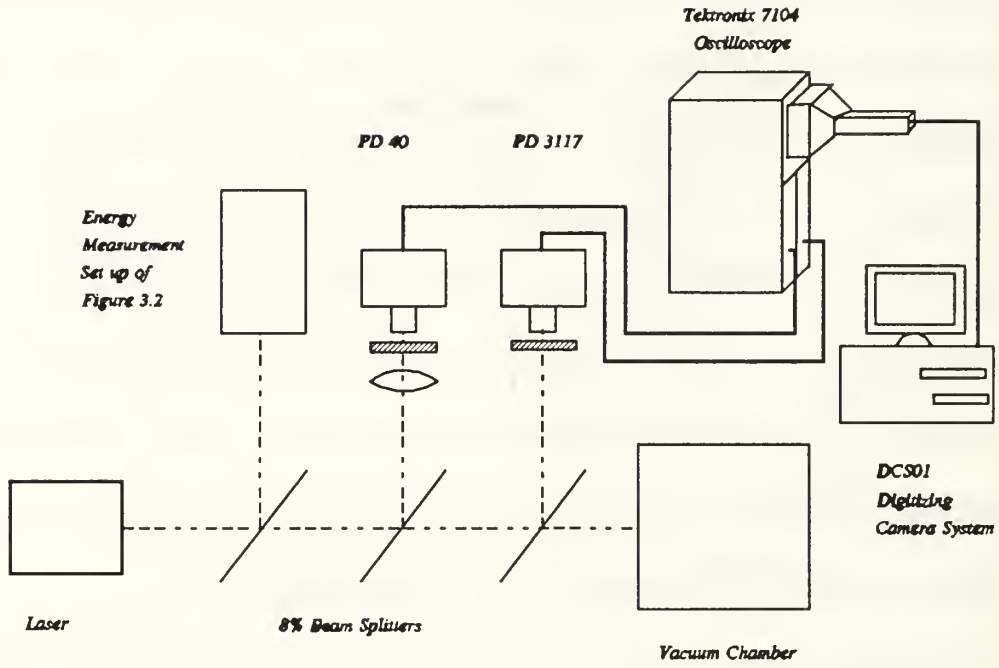

Figure 3.3. Arrangement for laser energy measurement with a photodetector.

Figure 3.4. By using the software available with the system, the output could be integrated. The result of integration for the pulse in Figure 3.4 is given in Figure 3.5. Simultaneously, the laser energy was measured with the calorimeter-micro voltmeter system. A typical output of this system is shown in Figure 3.6. Comparing the energy measured this way with the result of the integration, and repeating this procedure for a number of shots, a calibration factor was obtained. This factor was used to determine the energy of the laser pulse using the fast photodiode. The uncertainty of the measurement was determined to be 5%.

This method of laser pulse energy measurement allowed the laser to be shot every 2.5 minutes which was the minimum waiting time for the laser to cool down.

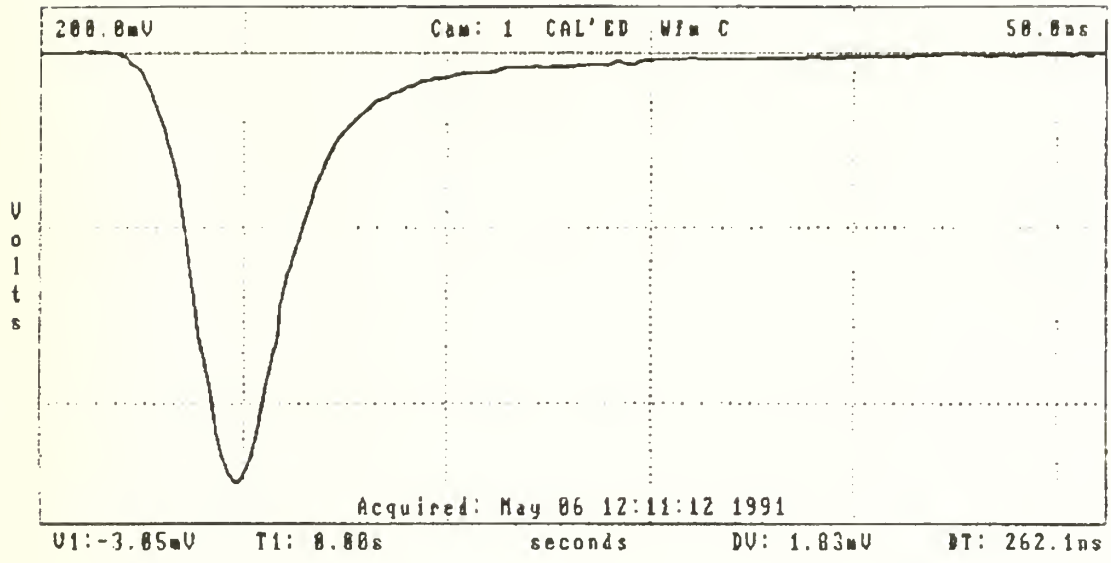

Figure 3.4. A typical laser pulse captured by DCS.

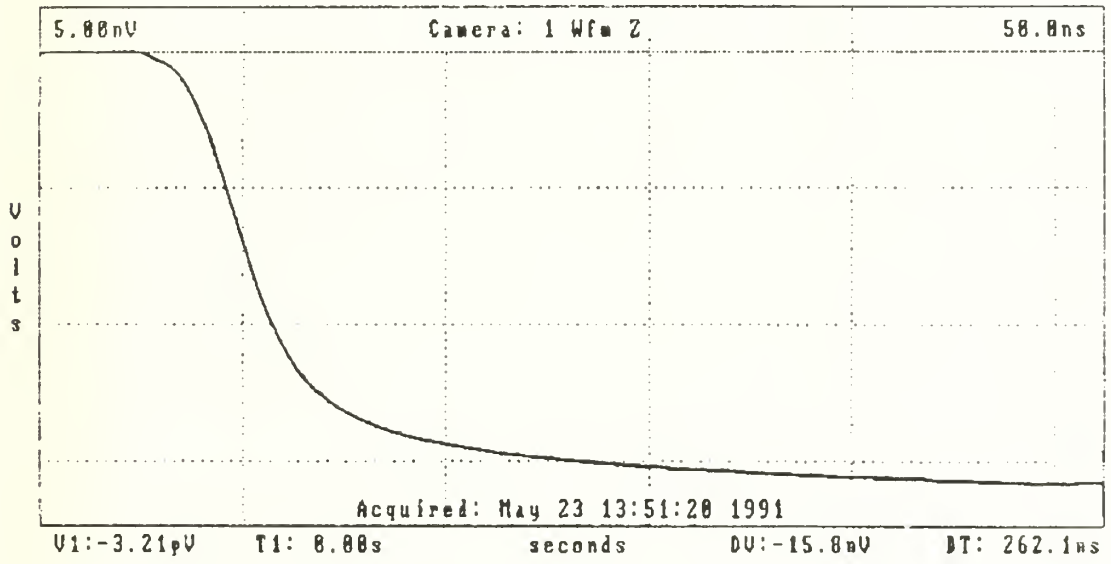

Figure 3.5. Integrated laser pulse of Figure 3.4.

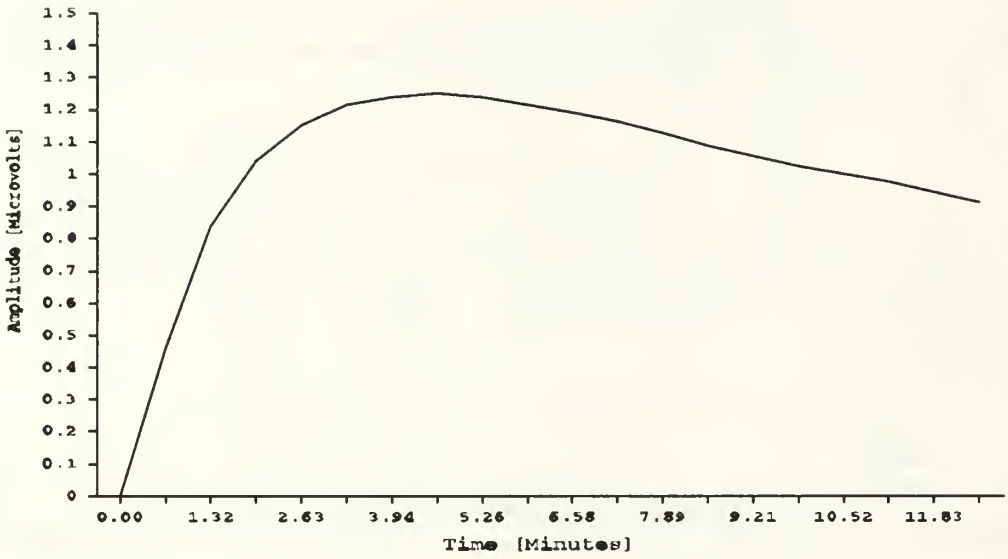

Figure 3.6. Rise and cooling curve of the calorimeter after the laser shot of Figure 3.4.

3. Ultra High Vacuum Chamber

The vacuum chamber in which the stainless-steel target was placed had a volume of 24 ± 2 liters. The material from which the chamber was built was Type 304 Stainless steel. A forepump was used to evacuate the chamber down to 10^{-2} torr which was necessary to start the turbo molecular pump which could evacuate the chamber down to a pressure of 10^{-8} Torr. The pressure inside the chamber was measured by a Veeco Type RG-3A Vacuum Gauge.

The laser beam was aligned 45 degrees from normal to the target surface. The cylindrical stainless-steel target, mounted on a target holder, was four mm thick and 50 mm in diameter. The target was large enough to shoot the laser a number of times without replacement. A probe was used to hold the mounting and to rotate the target

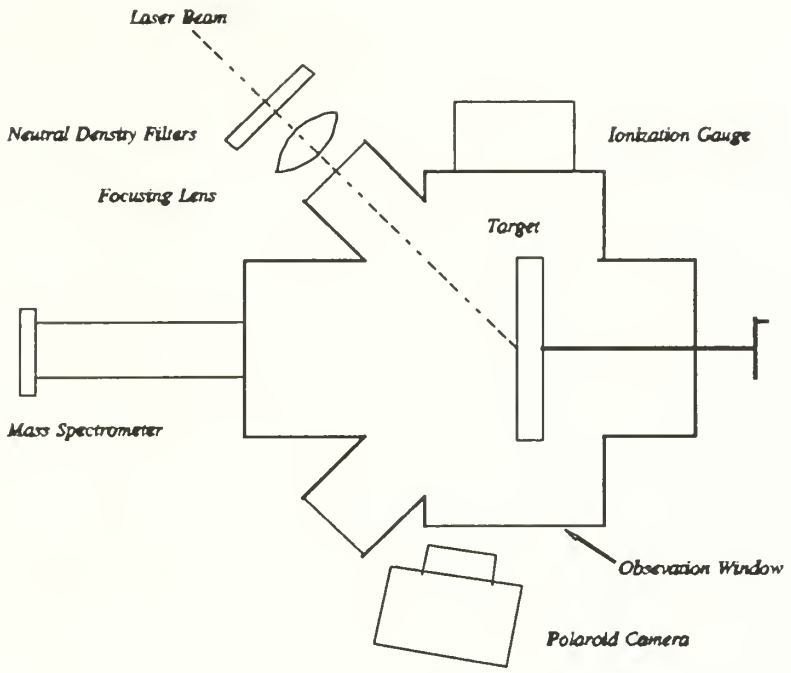

Figure 3.7. Diagram of the vacuum chamber used in the experiment.

whenever necessary without opening the chamber. Figure 3.7 is a diagram of the vacuum chamber. The target surface was viewed via the observation window by a polaroid camera which was placed 85 degrees from normal to the target surface, at a distance of 18.5 cm.

B. PROCEDURES

1. Target Preparation

The targets used for this study were type 304 stainless steel. They were first cleaned by an ultrasound cleaning system. Then, they were polished using standard metallurgical techniques with a final polishing slur of 1μm diamond paste.

2. Plasma Onset

The onset of plasma formation was determined for three different vacuum conditions. The first measurements were made at 10^{-8} torr which was the lowest pressure possible in the evacuated chamber. The laser was fired at 6-joule energy level, and the beam intensity on the target was varied by placing neutral density filters in the path. The focusing lens was placed behind the filters. Determination of actual plasma formation was made by taking still pictures of the target with a polaroid camera during the laser shot. The laboratory was darkened and the shutter was kept open during the shot.

The measurements at 10^{-6} torr and 10^{-4} torr were taken by letting air into the chamber while both pumps were running. The air leakage rate was adjusted by means of a bellow valve which was already a part of the vacuum chamber.

IV. EXPERIMENTAL RESULTS

A. PLASMA FORMATION

Before the results of the onset of the breakdown, several still pictures of plasma formation for several energy levels will be presented. These shots were made at a pressure of 10^{-8} torr. As explained in the previous chapter, the pictures were taken by a polaroid camera.

The first picture, Figure 4.1, was for a laser shot of 2.9×10^{-2} joules at the target focused to 19.1 mm^2. It shows a comparatively small volume of plasma formation. The following figures (Figures 4.2 to 4.5) include photographs of shots with increasing energy. The energy of each shot is given in the figure captions. As can be seen from the pictures, the more powerful the laser beam, the larger the volume of the plasma formed.

B. PLASMA ONSET

As stated before, the experiments were conducted under three different vacuum conditions: 10^{-4}, 10^{-6} and, 10^{-8} torr. The onset of plasma formation was determined by taking still pictures. If there was no plasma formation, then only a weak background light from the flash lamp of the laser was seen. If there was a small amount of plasma formation, it would be indicated by the light coming off the surface. The radiation resulted from excitation of neutrals and ions and recombination of the electrons and ions in the plasma cloud.

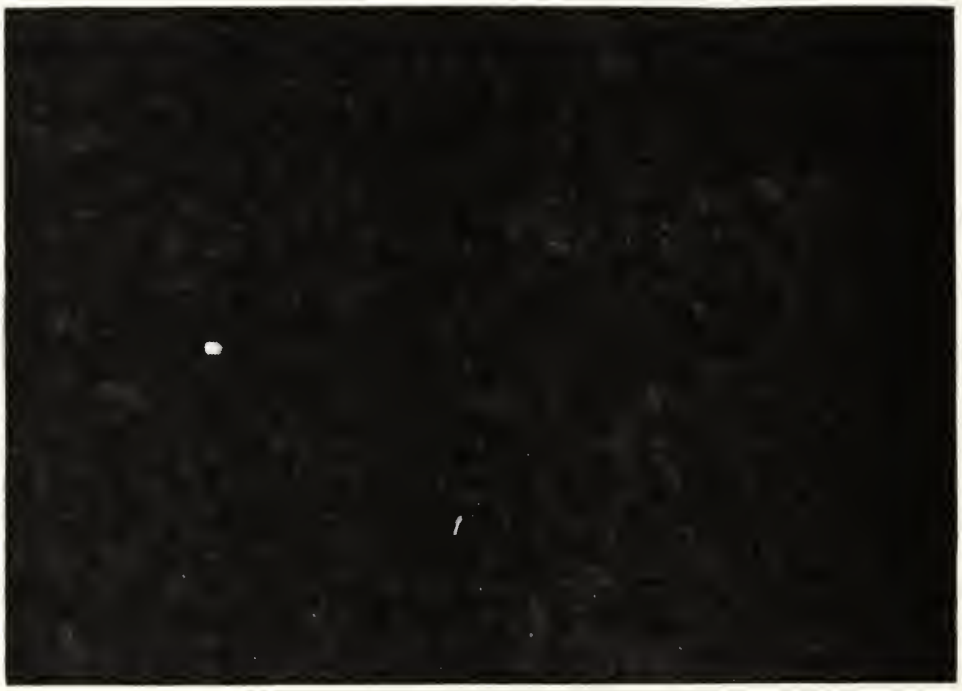

Figure 4.1. Plasma formation in a UHV chamber. (Energy = 2.9×10^{-2} joules)

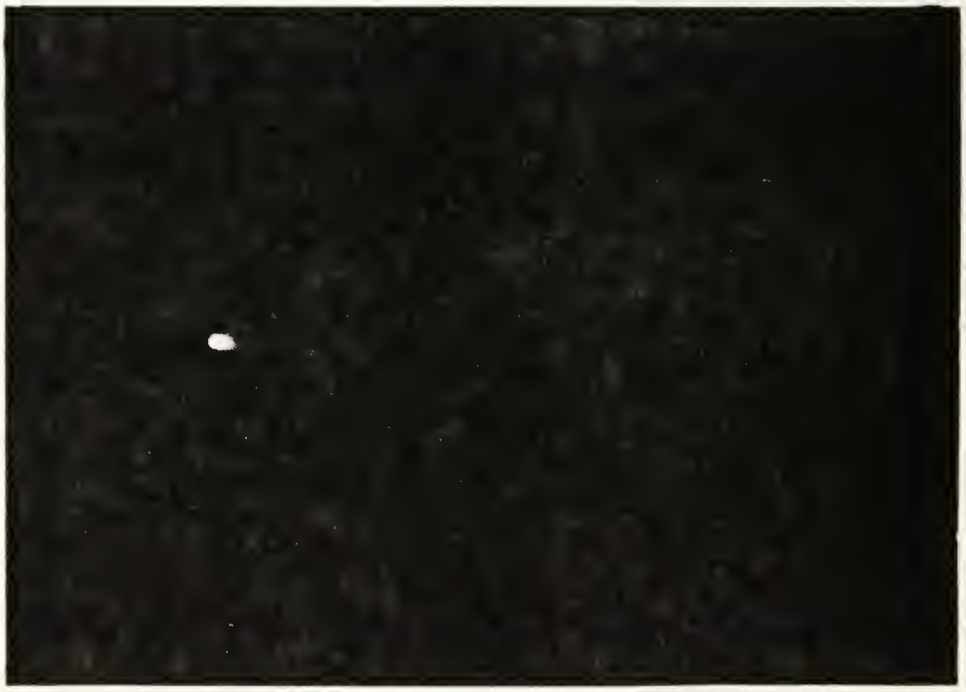

Figure 4.2. Plasma formation in a UHV chamber. (Energy = 3.2×10^{-2} joules)

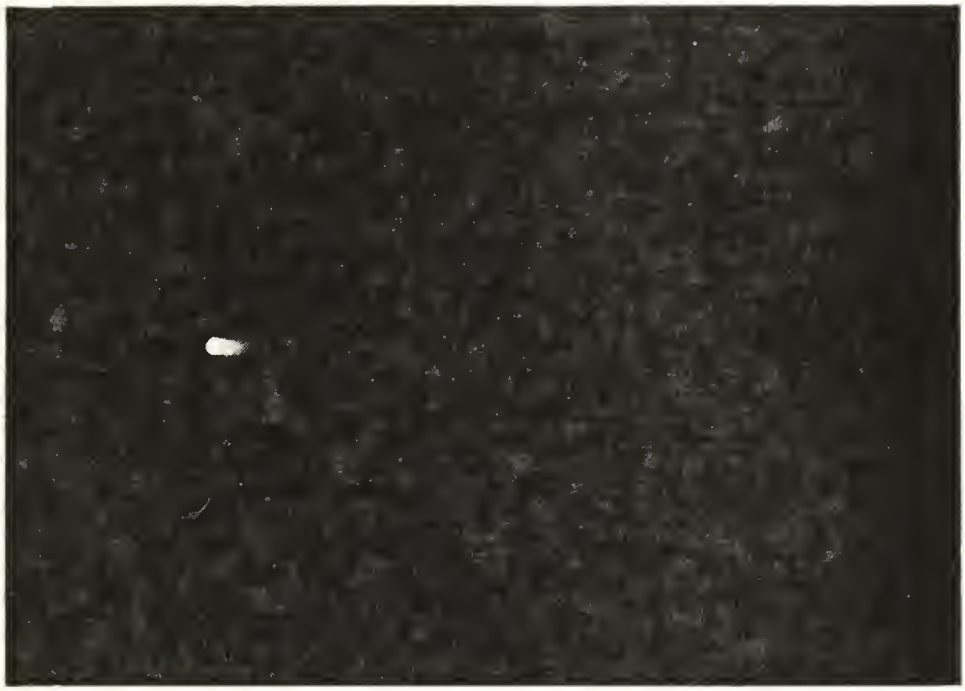

Figure 4.3. Plasma formation in a UHV chamber. (Energy = 3.7×10^{-2} joules)

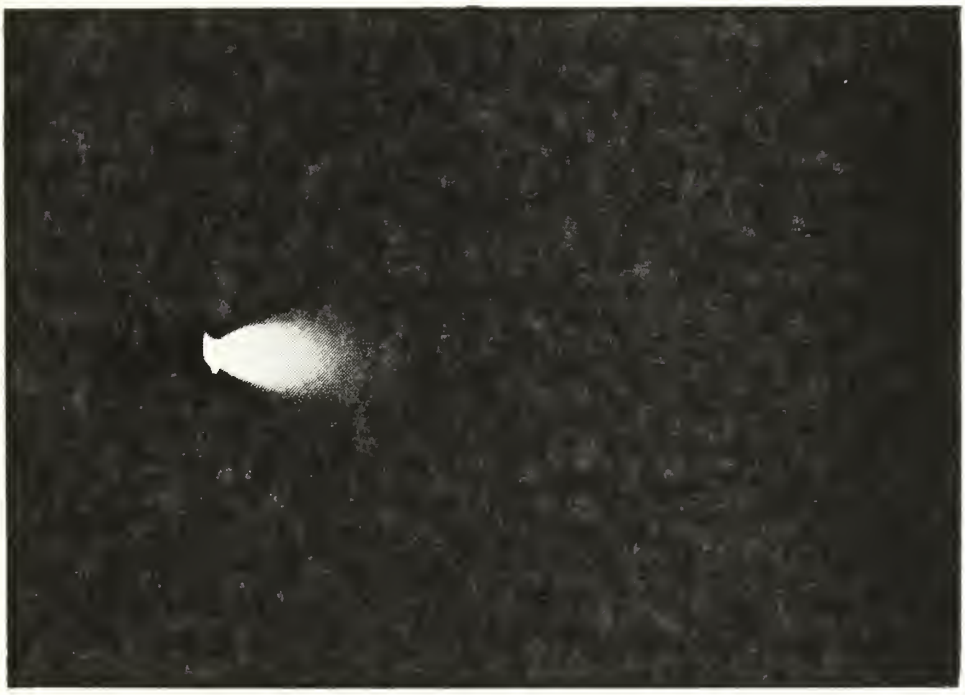

Figure 4.4. Plasma formation in a UHV chamber. (Energy = 1.1×10^{-1} joule)

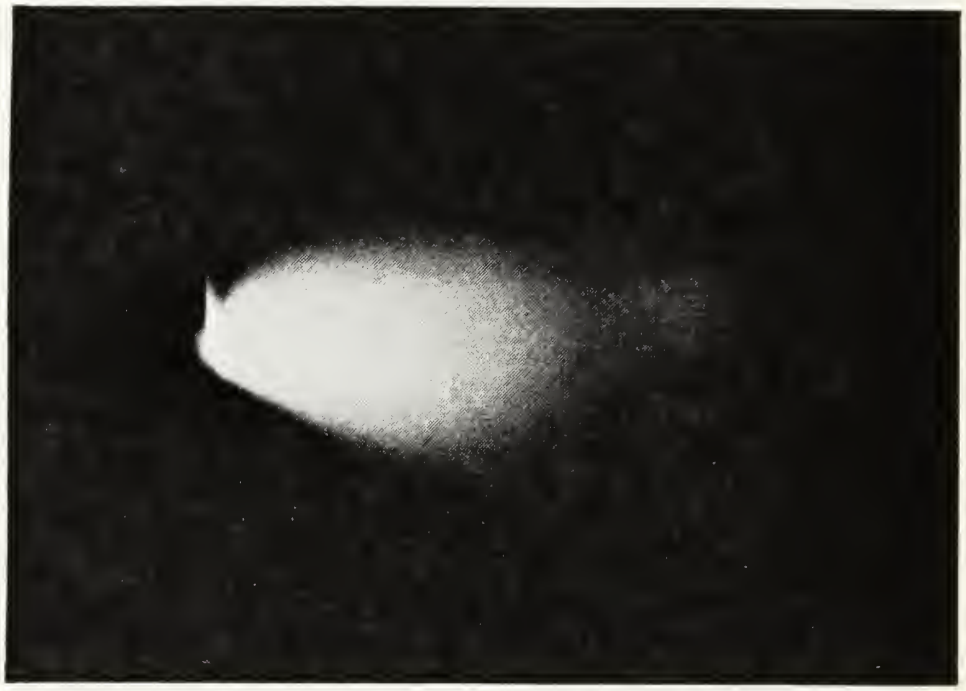

Figure 4.5. Plasma formation in a UHV chamber. (Energy = 2.3×10^{-1} joule)

First, the breakdown was studied at the 10^{-8} torr region. During the shots, the vacuum gauge was monitored to see if there is any rise in pressure. For relatively low energy levels at which the plasma formation was not probable, the vacuum gauge showed minimal pressure increases for a short time. Since the vacuum pumps were continuously pumping, the exact change in pressure could not be measured. A slight pressure increase was always observable even if there was no light emission. i.e., plasma formation. This is due to the desorption of contaminants from the laser heated spots on the metal surface. When there was plasma formation, the increase in pressure was higher. Reference 8 gives quantitative results for pressure changes in a vacuum chamber due to laser induced breakdown.

At the beginning, before taking the pictures, the metal surface was cleaned by 20 full power shots, without filters in the path. For those initials shots the energy of the beam was about six joules which corresponds to a power of 1.0×10^9 watts/cm^2 on the target. Then, several shots were fired at different energy levels and pictures were taken to determine the power level for plasma onset at a pressure of 10^{-8} torr. The experiments at 10^{-6} and 10^{-4} torr pressure were conducted at the same energy levels and under the same conditions.

The results of the three sets of measurements are presented by the chart given in Figure 4.6. "Plasma" and "no plasma" conditions are represented by "+"s and "o"s, respectively. The chart shows all data taken for the onset of plasma at different pressure levels. At 10^{-8} torr the transition between plasma and no-plasma occupies a relatively wide energy range: 2.2×10^{-2} - 3.7×10^{-2} joules. On the other hand, for 10^{-4} torr, the transition region is better defined and it occurs around 2.1×10^{-2} joules. For 10^{-6} torr, the transition is in between, 2.3×10^{-2} to 2.7×10^{-2} joules.

To determine an energy threshold for each vacuum level, the data was analyzed separately. The bar graph generated by using the data for 10^{-4} torr vacuum conditions is given in Figure 4.7. As can be seen from the figure, the threshold lies about 2.1×10^{-2} joules which corresponds to a power of 3.7×10^6 watts/cm^2 on the target. As it was pointed out before, the area of the focal point on the target was 19.1 mm^2. More than 50% of the shots created plasma were in the energy range of 2.0 - 2.5×10^{-2} joules. Below that level, the percentage of plasma formation was not significant.

The graphs for 10^{-6} and 10^{-8} torr are also presented in Figure 4.7. For 10^{-6} torr the threshold energy was $2.4x10^{-2}$ joules ($4.2x10^{6}$ watts/cm^2). Below $2.0x10^{-2}$ joules there was no plasma formation. In the $2.0\text{-}2.5x10^{-2}$ joule range, the percentage of shots causing plasma formation was less than 40%. Above that range more than 50% of the shots led the breakdown of the surface.

For 10^{-8} torr, the threshold was at $2.9x10^{-2}$ joules ($5.1x10^{6}$ watts/cm^{-2}). The transition from plasma to no plasma spread over a wider energy range. Less than 50% of the shots with energies below $2.5x10^{-2}$ joules led to breakdown. There was plasma formation for more than 50% of the shots with energies over $3.0x10^{-2}$ joules.

The number of monolayers formed after a laser shot at different pressures can be calculated by using equation (9). At 10^{-8} torr, approximately four minutes are necessary for a monolayer to form on the metal surface. Hence, at that pressure it is highly probable to have only a fraction of one monolayer adsorbed. However, in three minutes, at 10^{-4} and 10^{-6} torr, up to "7500" and "75" layers form respectively. Therefore, it is reasonable to conclude that plasma onset occurs more easily if the number of absorbed monolayers is higher.

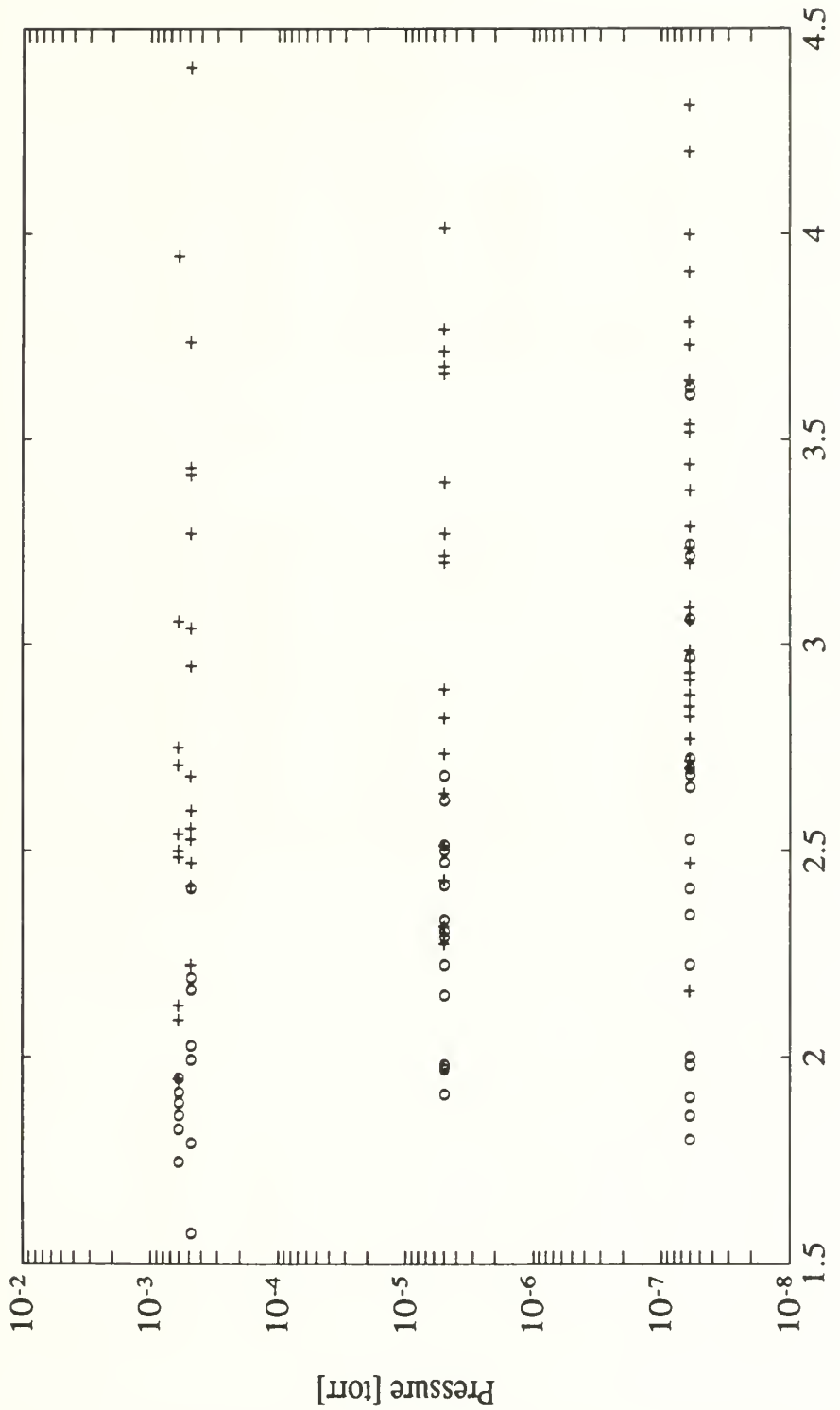

Figure 4.6. Onset of plasma at various pressures.

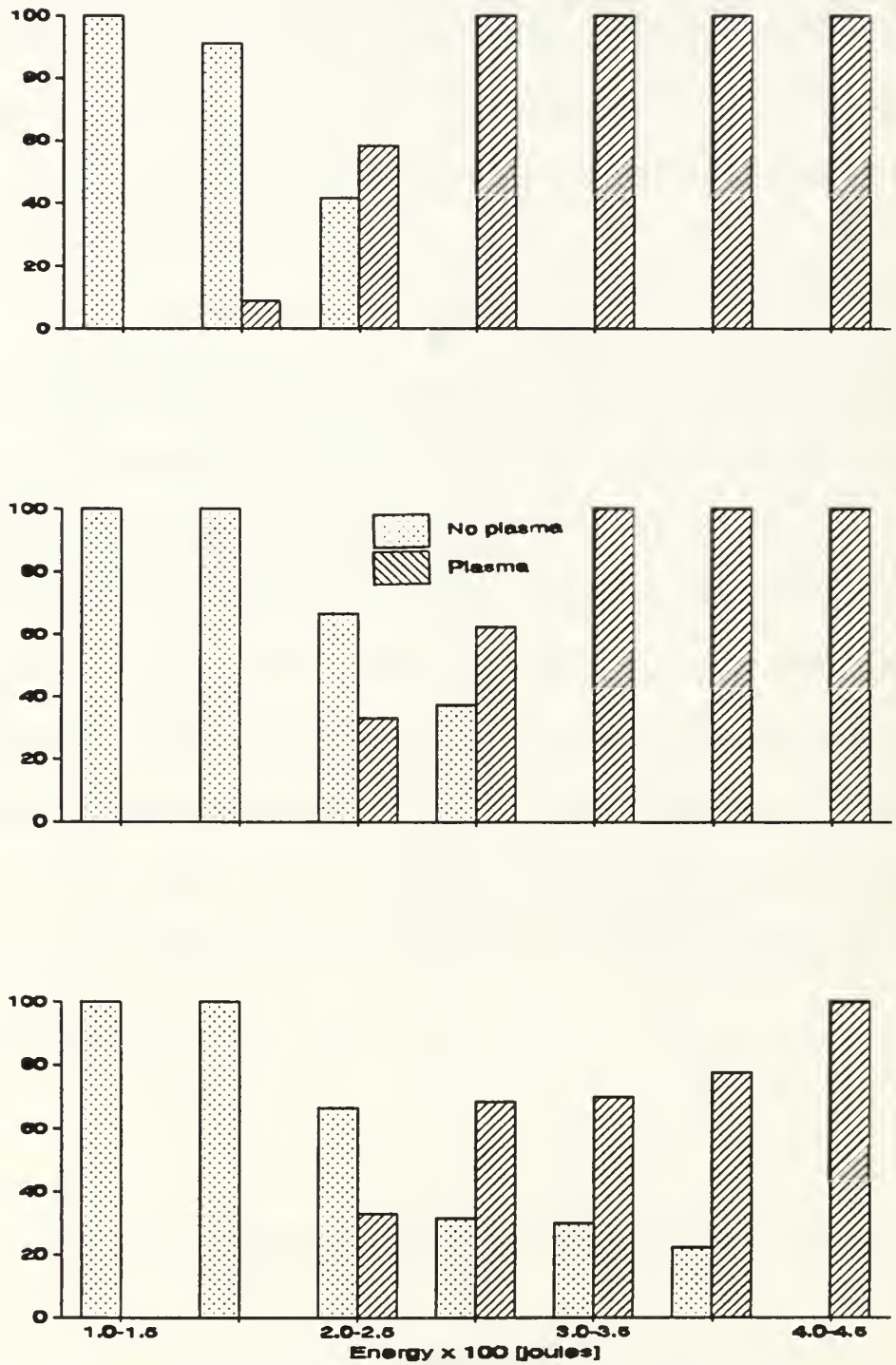

Figure 4.7. Plasma onset as a function of energy: $p = 10^{-4}$ (top), $p = 10^{-6}$ (middle), $p = 10^{-8}$ (bottom).

CONCLUSIONS

This report has described how laser induced breakdown occurs on a metal surface exposed for about three minutes to pressures ranging from 10^{-8} torr (ultra high vacuum) down to 10^{-4} torr. The laser power necessary for breakdown at different pressures were found to be different. The lower the pressure, the higher the laser power necessary to cause the breakdown.

The average power required for laser induced breakdown in vacuum for type 304 stainless steel was found to be of the order of 10^6 watts/cm^2. At 10^{-8} torr the power required for breakdown was around 5.1×10^6 watts/cm^2. It was 4.2×10^6 watts/cm^2 at 10^{-6} torr and 3.7×10^6 watts/cm^2 at 10^{-4} torr. The results agree with Schwirzke's model proposed for laser induced breakdown [Ref. 9]. The onset of breakdown occurs in the desorbed gas layers.

LIST OF REFERENCES

1. Radziemski, L. J., Cremers, D. A., *Laser-Induced Plasmas and Applications*, pp. 1-67, Marcel Dekker, Inc.,1989.

2. Schwirzke, F., "Laser-Plasma-Surface Interactions", *Laser Interaction and Related Plasma Phenomena, Vol. 8*, H. Hora and G. H. Miley, eds., p. 104, Plenum Publishing Corporation 1988.

3. *Vacuum Technology its Foundations Formulae and Tables*, pp. 34-35, Leybold-Heraeus Vacuum Products Inc.

4. Union Carbide Electronics, *KORAD Laser Systems Instruction Manual for Nd:Glass Laser*,Five Volumes, KORAD Department, Santa Monica, California 1969.

5. Union Carbide Electronics, *KORAD Laser Systems Instruction Manual for Model K-J Laser Calorimeter*, KORAD Department, Santa Monica, California 1969.

6. *Operations Manual for Series PD40 Ultra High Speed Photodetectors*, Opto-Electronics Inc., Oakville, Ontario Canada, June 1983.

7. Tektronix Inc., *Digitizing Camera System Operation Manual*, 1988.

8. Schwirzke, F., "Laser Induced Desorption of Gas from Metallic Surfaces", *Journal of Applied Physics, Vol. 46, No. 11*, November 1975.

9. Schwirzke, F., "Laser Induced Breakdown and High Voltage Induced Breakdown on Metal Surfaces' to be published as a chapter in a book: *Laser Interaction and Related Plasma Phenomena, Vol. 9*, H. Hora and G. H. Miley, eds., Plenum Publishing Corporation, forthcoming in 1991.

10. Chen, F. F., *Introduction to Plasma Physics and Controlled Fusion*, p. 351, Plenum Press, 1984.

INITIAL DISTRUBITION LIST

1.	Defense Technical Information Center Cameron Station Alexandria, Virginia 22304-6145	2
2.	Library, Code 0142 Naval Postgraduate School Monterey, California 93943-5002	2
3.	Dr. F. Schwirzke, Code PH/Sw Naval Postgraduate School Monterey, California 93943-5100	2
4.	Cpt. Abdullah Gedik Feneryolu sokak, 29/10 Etlik, Ankara TURKEY	1
5.	Kara Harp Okulu Kütüphanesi Bakanlıklar, Ankara TURKEY	1
6.	Orta Doğu Teknik Üniversitesi Kütüphanesi 06531 Ankara TURKEY	1
7.	Boğaziçi Üniversitesi Kütüphanesi Arnavutköy, İstanbul TURKEY	1
8.	Hacettepe Üniversitesi Kütüphanesi Beytepe, Ankara TURKEY	1
9.	Ankara Üniversitesi Fen Fakültesi Kütüphanesi Beşevler, Ankara TURKEY	1
10.	Bilkent Üniversitesi Kütüphanesi Beytepe, Ankara TURKEY	1
11.	Deniz Harp Okulu Kütüphanesi Tuzla, İstanbul TURKEY	1

12. Hava Harp Okulu Kütüphanesi
Yeşilyurt, İstanbul TURKEY 1

Thesis
G2575
c.1

Gedik
Energy threshold for laser induced breakdown on a metal surface under high and ultra high vacuum conditions.